Molecular Mechanism of Peroxisome Proliferator-Activated Receptor alpha Activation by WY14643: a New Mode of Ligand Recognition and Receptor Stabilization

Bernardes, Amanda; Telles de Souza, Paulo C; Muniz, João R C; Ricci, Clarisse G; Ayers, Stephen D; Parekh, Nili M; Godoy, André S; Trivella, Daniela B B; Reinach, Peter; Webb, Paul

Published in:
Journal of Molecular Biology

DOI:
10.1016/j.jmb.2013.05.010

jmb Article

Molecular Mechanism of Peroxisome Proliferator-Activated Receptor α Activation by WY14643: a New Mode of Ligand Recognition and Receptor Stabilization

Amanda Bernardes[1], Paulo C. T. Souza[2], João R. C. Muniz[1], Clarisse G. Ricci[2], Stephen D. Ayers[3], Nili M. Parekh[4], André S. Godoy[1], Daniela B. B. Trivella[5], Peter Reinach[4], Paul Webb[3], Munir S. Skaf[2] and Igor Polikarpov[1]

*1 - **Institute of Physics of São Carlos,** University of São Paulo, Avenida Trabalhador Sãocarlense 400, São Carlos, SP 13560–970, Brazil*
*2 - **Institute of Chemistry,** University of Campinas, Cx. P. 6154, Campinas, SP 13084–862, Brazil*
*3 - **Diabetes Center and Cancer Research Unit,** The Methodist Hospital Research Institute, Houston, TX 77030, USA*
*4 - **Department of Biological Sciences,** College of Optometry, State University of New York, 33 West 42nd Street, New York, NY 10036, USA*
*5 - **National Center for Research in Energy and Material,** Natinal Biosciences Laboratory, 13083-100 Campinas, SP*

***Correspondence to Igor Polikarpov:** ipolikarpov@ifsc.usp.br*
http://dx.doi.org/10.1016/j.jmb.2013.05.010
Edited by S. Khorasanizadeh

Abstract

Peroxisome proliferator-activated receptors (PPARs) are members of a superfamily of nuclear transcription factors. They are involved in mediating numerous physiological effects in humans, including glucose and lipid metabolism. PPARα ligands effectively treat dyslipidemia and have significant antiinflammatory and anti-atherosclerotic activities. These effects and their ligand-dependent activity make nuclear receptors obvious targets for drug design. Here, we present the structure of the human PPARα in complex with WY14643, a member of fibrate class of drug, and a widely used PPAR activator. The crystal structure of this complex suggests that WY14643 induces activation of PPARα in an unusual bipartite mechanism involving conventional direct helix 12 stabilization and an alternative mode that involves a second ligand in the pocket. We present structural observations, molecular dynamics and activity assays that support the importance of the second site in WY14643 action. The unique binding mode of WY14643 reveals a new pattern of nuclear receptor ligand recognition and suggests a novel basis for ligand design, offering clues for improving the binding affinity and selectivity of ligand. We show that binding of WY14643 to PPARα was associated with antiinflammatory disease in a human corneal cell model, suggesting possible applications for PPARα ligands.

Introduction

The peroxisome proliferator-activated receptors (PPARs) are members of the nuclear receptor superfamily, a group of ligand-inducible transcription factors[1] involved in the regulation of important and diverse biological processes.[2] They share a common structural organization, composed of a variable N-terminal domain harboring a ligand-independent activation function, a conserved DNA-binding domain (DBD) and a C-terminal ligand-binding domain (LBD), which contains the ligand-dependent activation function 2 (AF-2).[3] Apart from ligand recognition and binding, the LBD has additional functions such as (i) regulating interactions with cofactors involved in signal transduction during transcription and (ii) binding to homodimerization or heterodimerization partners.[4,5]

PPARα is one of three PPAR subtypes (PPARα, PPARβ/δ and PPARγ), each of which exhibit distinct tissue expression patterns and regulate diverse biological functions, mediated by activation upon binding of their respective ligands.[6,7] PPARα is predominantly expressed in the liver and, to a lesser extent, in other cell types, including macrophages, smooth muscle and endothelial cells. In these cells,

PPARα plays a critical role in lipid metabolism including β-oxidation of fatty acids and energy homeostasis.[8] Additionally, it has antiinflammatory and anti-thrombotic actions.[9,10]

Many synthetic and natural PPAR ligands have been identified,[11] and three-dimensional structures of ligands bound to this receptor class provided some understanding of the structural basis for the mode of action.[12] Activation of PPARα by agonist ligands triggers conformational changes in PPARα—including stabilization of the extreme C-terminal H12 (AF-2 helix) in an active position—and enhances heterodimerization with the retinoid X receptor,[13] promoting recruitment of nuclear receptor coactivators and ultimately gene transcription.[14,15]

Less clear are determinants that influence affinity of ligands for PPARα. Several fibrates—that are PPARα agonists—are used to treat dyslipidemia and hypertriglyceridemia[16] or combined with other drugs in antidiabetic therapies.[17] These, however, only exhibit weak affinities for PPARα, and there is interest in new fibrates or fibrate analogs with improved potency and selectivity for PPARα.[18] Pirinixic acid (also known as WY14643), a fibrate analog that was used as an anti-hypercholesterolemic agent[19] and responsible for promoting peroxisome proliferation,[20] is a potent and selective PPARα ligand.[21] Despite its wide-ranging use as a research tool for studies of PPARα, its binding mode and reasons for improved affinity have not been resolved.

PPARα also regulates inflammatory responses.[22,23] PPARα ligands display potential antiinflammatory properties in atherogenesis and hepatitis.[24] In ocular tissue, chronic inflammation resulting from corneal epithelial injury and/or infection can result in loss of tissue transparency and compromised vision.[25] At present, there has been no evaluation of PPARα ligand effects in corneal inflammation models. Recent studies have demonstrated that WY14643 may be a pro-inflammatory agent rather than antiinflammatory, possibly preventing therapeutic application in ophthalmology.[26] Furthermore, in rabbit corneal epithelium, WY14643 is involved in regulation of hypoxia-induced inflammation by lowering of cellular GSH levels.[27] Further analyses are necessary to discern the viability of PPARα agonists as ophthalmic antiinflammatory agents.

In this paper, we present a crystal structure of PPARα LBD complexed with WY14643, refined to a resolution up to 2.5 Å. This structure shows that ligand interacts with H12, which supports the agonist behavior of WY14643 and conforms with the classic activation hypothesis.[28] Unexpectedly, a second molecule of WY14643 occupies a different position in the ligand binding pocket. Functional analysis, combined with site-directed mutagenesis and molecular dynamics (MD) simulations, suggests a biological role for this second binding site. We investigated the effect of WY14643 in expression of a representative pro-inflammatory cytokine (IL-6) and a chemoattractant (IL-8) in corneal epithelial cells in response to hypertonic stress shown to induce inflammation *in vivo* and *in vitro*. WY14643 inhibition of stress-induced IL-6 and IL-8 expression points to the possibility that WY14643 may have therapeutic value in corneal inflammation in a clinical setting.

Results

Crystal structure shows two molecules of WY14643 anchored to PPARα LBD

WY14643 is widely known as a potent PPARα agonist. To gain further insight into its binding mode, we co-crystallized WY14643 with the human PPARα LBD and solved the structure with a resolution up to 2.5 Å, sufficient for building protein and ligand atomic models. The PHENIX.XTRIAGE program[29] identified twinning in the data set with a fraction of 39% and k, h, −l as a twinning operator. This information was used during the refinement process.

Table 1. Data collection and refinement statistics

	PPARα + WY14643
Data collection	
Space group	$P2_12_12_1$
Unit cell dimensions (Å)	62.39, 62.68, 180.05
Resolution (Å)	36.56–2.51 (2.65–2.51)
Number of frames	370
Number of unique reflections	22,365
Δϕ (°)	0.25
Mosaicity	0.66
Multiplicity	3.6 (3.5)
Completeness (%)	89.9 (98.7)
R_{merge} [a]	0.104 (0.497)
$I/\sigma(I)$	7.7 (2.1)
Refinement	
Reflections	22,323
R_{work}/R_{free} [b] (%)	17.31/21.57
Number of atoms	
Protein (two molecules)	4092
Ligands (four molecules)	84
Water	62
B-factors	
Protein (two molecules)	47.11
Ligands (four molecules)	48.57
Water	37.02
RMSD	
Bond lengths (Å)	0.011
Bond angles (°)	1.350
Ramachandran outliers	0

Values in parentheses refer to the outer shell (2.05–1.95 Å).

[a] $R_{merge} = \sum hkl \sum i |I_i(hkl) - \langle I(hkl)\rangle| / \sum hkl \sum i I_i(hkl)$, where $\langle I(hkl)\rangle$ is the mean $I(hkl)$ over symmetry-equivalent reflections.

[b] $R_{factor}/R_{free} = \sum hkl ||F_{obs}| - |F_{calc}|| / \sum hkl |F_{obs}|$, where F_{obs} and F_{calc} are the observed and calculated structure factors, respectively. R_{free} was calculated using 5% of the total reflections, which were chosen randomly and omitted from the refinement.

The final model consists of two monomers of hPPARα LBD in the asymmetric unit (encompassing the amino acid residues from T200 to M467), four molecules of the ligand WY14643 and 62 water molecules. All protein residues were found in allowed regions of the Ramachandran plot, and the validation parameters exhibited the quality of final models. Refinement statistics are given in Table 1.

Both macromolecular chains displayed an overall fold in agreement with that of other LBD nuclear receptor structures.[18,30,31] They are mainly composed of helices, arranged into a three-layered sandwich, with the C-terminal AF-2 helix (H12) positioned in the active conformation, consistent with the agonist nature of the WY14643 ligand (Fig. 1a).

The protein–ligand interactions observed in chains A and B were basically the same, with two molecules of WY14643 bound to each LBD. Consequently, the two complexes present in the crystal asymmetric unit will be treated hereafter as a generic model (Fig. 1a). This is the first PPARα solved structure showing two molecules within the ligand binding pocket. One of the WY14643 molecules occupies standard PPARα agonist position, performing polar and hydrophobic contacts with the protein. Residues S280 (H3), Y314 (H5), H440 (H11) and Y464 (H12) form a well-recognized hydrogen-bonding network with the ligand carboxylic acid (Fig. 1b). In addition to these standard carboxylate interactions with the upper part of the PPARα binding pocket, WY14643 also makes several hydrophobic contacts with the lower part of the pocket (Fig. 1b), involving residues C276, T279, I317 and M330. As identified for other PPAR agonists,[32] the hydrogen bond involving Y464 is very important for maintaining the protein active conformation; Y464 is located on the inner surface of the AF-2 helix (H12) and the closed conformation of the AF-2 helix is crucial for regulation of coactivator recruitment.[28]

The second WY14643 binds to a secondary site positioned between H2′ and H3. This region is called Ω-loop; it is usually poorly structured and is thought to be a very flexible region of LBD but appeared very well ordered here. This second ligand is primarily stabilized by nonpolar interactions with I241, L247

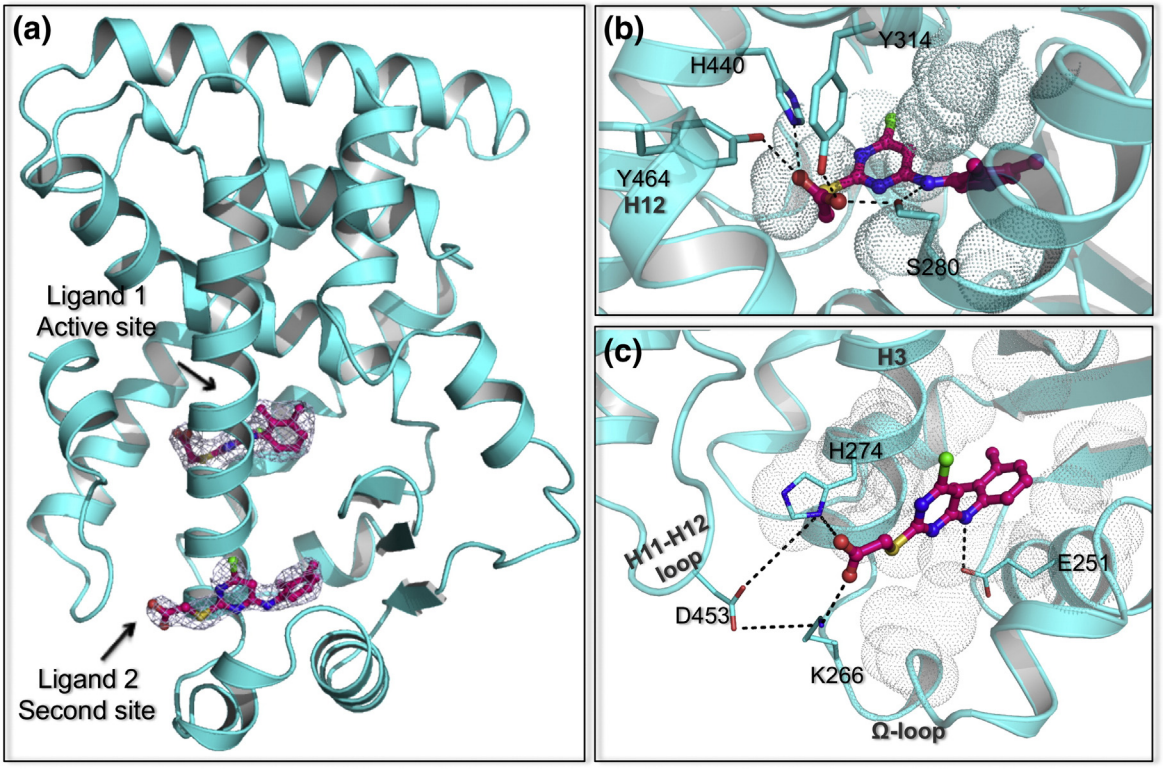

Fig. 1. hPPARα LBD crystal structure bound to two WY14643 molecules. (a) LBD receptor indicating the region of the first and second sites. Both WY14643 molecules fitted into the electron density map calculated using omit map methodology by PHENIX program. (b) Details of interactions in the first site. The ligand head carboxyl group making interactions with the polar side chains, including Y464, which result in the PPAR LBD conventional active conformations of helix 12. (c) Ligand and residue interactions occurring in the newly identified second site and residues involved in a salt bridge network between important protein regions. Black broken lines represent hydrogen bonds and dotted circles denote residues involved in hydrophobic interactions.

(H2′), V255, I263, R271 (H3), I272 (H3), H274 (H3) and C275 (H3), which contact the fused heterocyclic rings. Another contributor to stabilization are salt bridges between (i) the nitrogen located in the ligand central region and E251 (H2′) and (ii) between the carboxylic group of the ligand and the residues K266 (Ω-loop) and H274 (H3) (Fig. 1c). These basic residues can also interact with D453 (loop H11–H12), as suggested by the MD simulations discussed later, and form a salt bridge network, which connects the Ω-loop, H3 and the H11–H12 loop.

Y314 is likely to promote PPARα selectivity of WY14643

WY14643 binds to human PPARα receptor with high affinity and selectivity.[24,33] The ligand selectivity for PPARα was confirmed in dose–response curves obtained from cell-based assays with the three PPAR subtypes (Fig. 2). Consistent with previous observations,[34–36] WY14643 displayed higher potency in activating PPARα with an EC_{50} value of 5.38 μM. On the other hand, the PPARβ and PPARγ curves did not reach a plateau level, which precluded calculation of ligand potency with these subtypes (PPARδ/β EC_{50} = 26 mM and PPARγ EC_{50} = 17 mM) (Fig. 2a).

To identify possible molecular determinants of WY14643 selectivity, we set out to define unique PPARα amino acids that might be involved in ligand contact among residues that are conserved between all three PPARs.[31] To do this, we carried out a comparison of the three-dimensional structures of the subtypes by superposition of crystal structures [Protein Data Bank (PDB) IDs 3ET2 (PPARβ) and 3ET0 (PPARγ)] and alignment of their backbones. Among residues involved in polar contacts with the first ligand molecule, αY314 is replaced by βH287 and γH323 (Fig. 2b). This single amino acid substitution is also responsible for the selectivity for other ligands.[31,37] No significant PPAR subtype differences in amino acids involved in contact with the second ligand were observed.

αY314 and ligand oxygen atom contacts further stabilized the ligand into the PPARα binding site. A possible role for αY314 in PPARα selective binding of WY14643 is corroborated by previous structure–activity relationship studies, which showed that bulky aromatic residues attached to α-position of the carboxylic group of WY14643 reduced PPARα selectivity and increased PPARγ binding.[38] The described change in preference of PPARγ for compounds with bulky α-residues can be similarly explained by the same residue substitution cited above (αY314–γH323).[31] In the PPARα pocket, tyrosine occupies more space and impairs the accommodation of large substituents. Smaller ligands, however, are able to form tighter interactions with PPARα than in the larger PPARγ pocket. Variations in the pocket topology and hydrophobicity may also contribute to selectivity; the PPARα isotype pocket is more hydrophobic than other PPARs,[31] and this may account for enhanced interactions between the hydrophobic tail of WY14643 and PPARα.

The second site is important for function

The presence of a second ligand molecule at an unsuspected position in the PPARα LBD raises

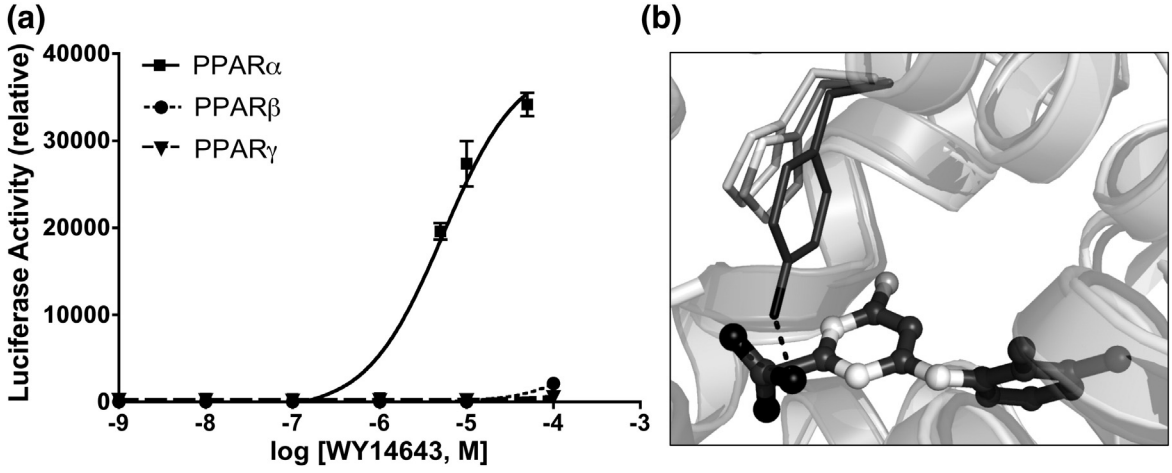

Fig. 2. The transcription activity of WY14643 tested toward three PPAR LBD subtypes in GAL4-based assays. (a) Tests are showed in the concentration–response curves and the ligand activation expressed as a relative luciferase activity. All assays were performed in three replicates and were normalized by *Renilla* luciferase activity. (b) Superposition of crystal structures of PPARα + WY14643, PPARβ (PDB ID 3ET2) and PPARγ (PDB ID 3ET0). This analysis showed the substitution of αY314 (dark gray) by βH287 (gray) and γH323 (light gray), suggesting its role in the isotype α selectivity.

questions about second-site functionality: does the second ligand merely stabilize PPARα in the crystalline form or is this ligand also necessary for generating conformational changes required for the full PPARα activity? One indication of second-site functionality is that this region can also be partially occupied by other high-affinity synthetic PPARα ligands[18,30–32,39–43] and partial agonists in PPARγ.[44–46] PPARγ partial agonists that occupy this position cause conformational changes that produce a decrease in the helix 12 dynamics and stabilize the interaction with coactivators.

We carried out site-directed mutagenesis to explore the function of the receptor second binding site. The selected mutation (V255A/I263A) should disrupt ligand binding to his region, without altering the first site by decreasing ligand hydrophobic contacts (Fig. 3a). Effects of mutations upon WY14643 activity were compared with that of the high-affinity synthetic ligand GW7647, which served as a positive control of PPARα functionality and should interact only with the first site. Table 2 shows differences in EC_{50} values for native and mutant protein constructs. The PPARα V255A/I263A mutant decreased PPARα sensitivity to WY14643 (Fig. 3b). It was not possible to extract the EC_{50} value for this ligand since the titration curves do not reach a plateau. On the other hand, these mutations did not affect the activity of GW7647 whose EC_{50} value was practically the same for both native and mutated PPARα. This invariance shows that the mutant protein remained active because its folding was unaffected and suggests that the second site is required for full WY14643 activity.

Table 2. Potency of WY14643 and GW7647 (control) toward PPARα and mutants, as determined in GAL4-based assays

Clone of PPARα	EC_{50} (M) (WY14643)	EC_{50} (M) (GW7647)
Wild type	5.38×10^{-6}	8.13×10^{-8}
V255A/I263A	~0.73 (ambiguous)	5.27×10^{-8}

Values were calculated from three independent experiments each performed in triplicate.

WY14643 interactions in the second site promote a local stabilization of the LBD and AF-2 region

Binding of WY14643 to the second binding site could activate PPARα by stabilizing the H12 in the active conformation without any direct contact with the helix, analogous to PPARγ partial agonists.[44–46] Additional interactions in the second site between WY14643 and residues near H12 were detected in the crystallographic model. H274 (H3) and K266 (Ω-loop) form salt bridges with the carboxylate group of the second WY14643 molecule. These residues are also close to D453 (loop H11–H12).

The roles of H264, K266 and D453 on WY14643 binding and activation were investigated via site-directed mutagenesis followed by transactivation

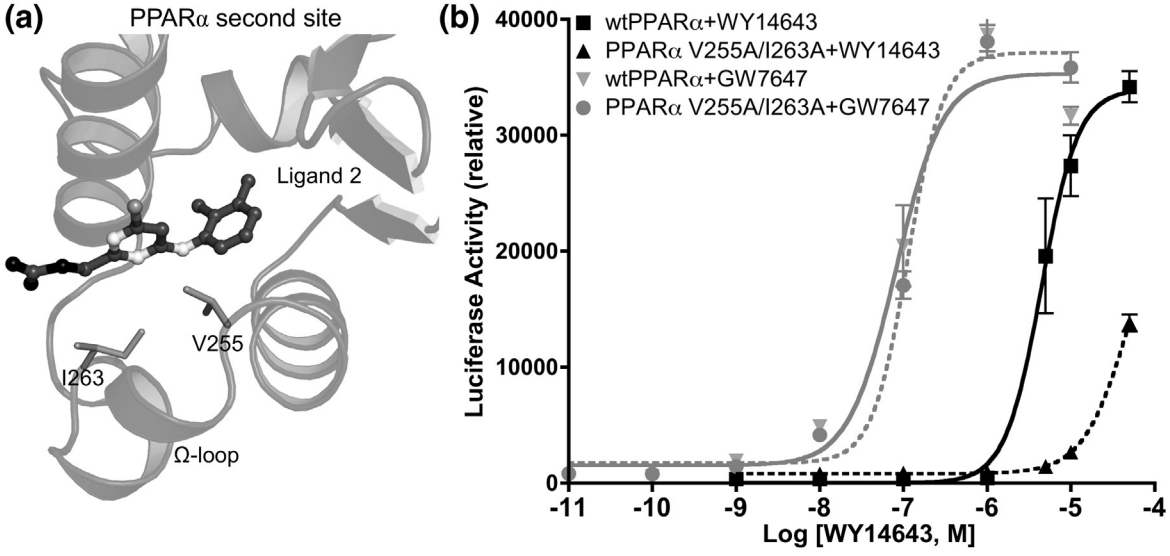

Fig. 3. Double mutation (V255A/I263A) effect on the PPARα activity against WY14643. (a) The V255 and I263 residues that were mutated to alanine. Both residues are located in the protein second site. (b) The transcription activity of WY14643 (black lines) and GW7647 (used as a control; gray lines) were tested toward wild-type (continuous line) and mutated (broken line) PPARα in a GAL4-based assay. Results are expressed as a relative luciferase activity. All assays were performed in three replicates and were normalized by *Renilla* luciferase activity to remove differences in transfections efficiency.

Table 3. Potency of WY14643 and GW7647 (control) toward PPARα and mutants involving electrostatic interactions cluster, as determined in GAL4-based assays

Clone of PPARα	EC_{50} (M) (WY14643)	EC_{50} (M) (GW7647)
Wild type	0.67×10^{-6}	2.32×10^{-8}
H264A	3.31×10^{-6}	4.38×10^{-8}
K266A	2.20×10^{-6}	3.92×10^{-8}
D453A	2.18×10^{-6}	5.58×10^{-8}

Values were calculated from experiments performed in triplicate.

assays. Effects in the GW7647 activity were also investigated as a control to determine whether mutations influence actions of a ligand that only binds in the first site. All the selected residues were mutated to alanine in order to prevent the formation of electrostatic interactions. While mutations did not significantly affect efficacy of either ligand at high doses, they did reduce the potency of both WY14643 and GW7647, as observed in a shift in EC_{50} values (Table 3). Interestingly, however, the shift in EC_{50} values was larger with WY14643, which binds at the second site near the charge cluster, than with GW7647. Thus, the charge cluster is required for optimal ligand activation, probably because differences in the hydrophobic packing of Ω-loop and loop H11–H12 could affect H12 dynamics and inhibit ligand activation. However, the fact that charged residues play a more important role with WY14643 suggests that these interactions could become more important for ligands that bind at the second site.

To confirm this hypothesis, we performed two sets of MD simulations of the PPARα LBD: a set of six independent MD simulations with two WY14643 molecules bound to PPARα LBD and another set of six independent MD simulations with a single WY14643 molecule bound to the first site of PPARα LBD to test whether there were differences in mobility and/or stability of PPARα LBD structure with two ligands or one ligand.

Figure 4 shows aligned snapshots extracted from the simulations and the corresponding root-mean-square fluctuation (RMSF) as indicators of the mobility of the PPARα LBD. The alignment procedure is described elsewhere.[47,48] The presence of WY14643 at the second site strongly stabilizes the Ω-loop and the loop between H2 and H2′ (Fig. 4a) as compared to the presence of a single ligand at the

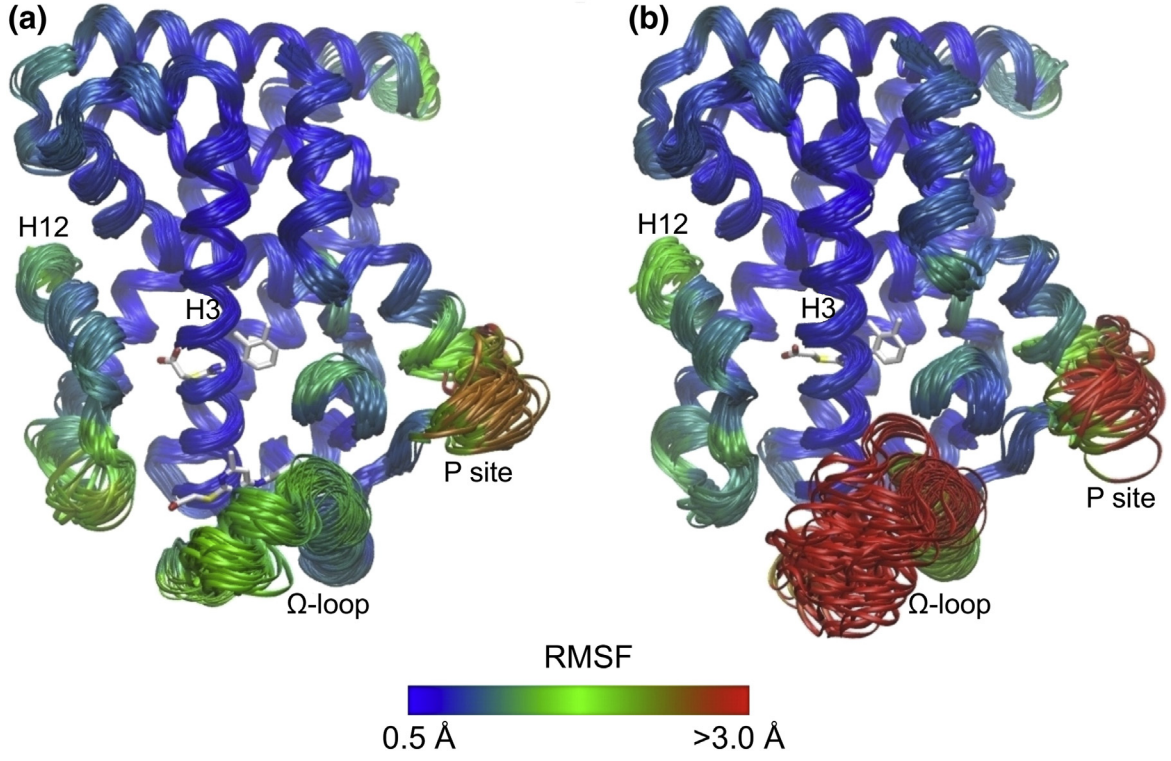

Fig. 4. Influence of the second WY14643 molecule on the mobility (RMSF of C^{α} atoms) of PPARα LBD backbone. The mobilities are shown as aligned snapshots from the MD trajectories and also as a color scale in which blue is low mobility (RMSF ≤ 0.5 Å), green is intermediate mobility (RMSF = 1.75 Å) and red is high mobility (RMSF ≥ 3.0 Å). These results suggest that PPARα LBD is stabilized by the presence of an extra ligand at the second site (a) as compared to PPARα LBD in the presence of a single ligand (b). Major mobility differences are observed at the Ω-loop, at the loop connecting H2 and H2′ (P site) and at the H12.

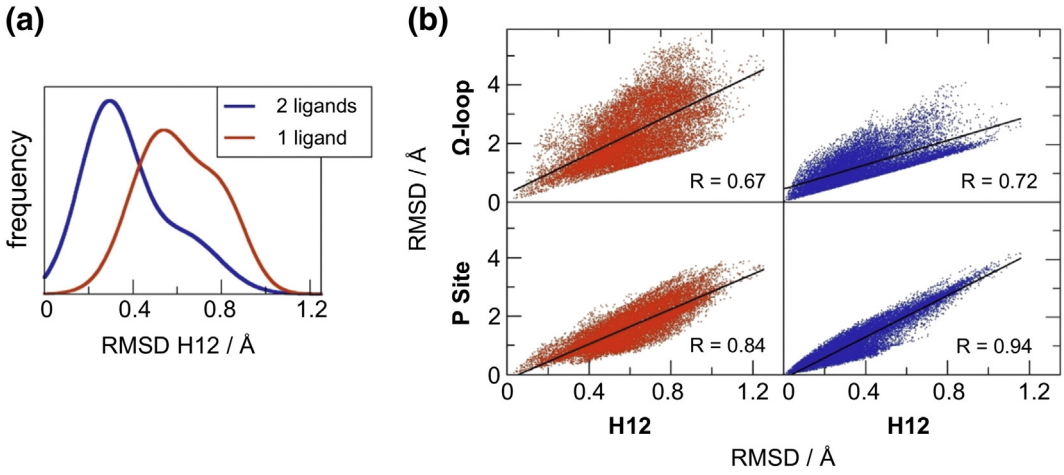

Fig. 5. H12, Ω-loop and P site mobilities computed for the essential trajectories. (a) RMSD distribution of H12 computed with respect to its average structure, showing the lower mobility of this helix in the presence of two ligands (blue) as compared to that in the presence of a single ligand (red). (b) RMSD of the H12 plotted against the RMSD values of Ω-loop and P site computed for the essential trajectories. There is a positive linear correlation between the mobilities of these regions, as confirmed by the correlation coefficients (*R*) resulting from linear regression analysis. These coefficients systematically increase in the presence of two ligands (blue) in comparison to just one ligand (red). There is no evident correlation between the Ω-loop and the P site in the presence of a single ligand ($R = 0.24$), but they appear to become slightly correlated in the presence of the second ligand ($R = 0.55$) (data not shown).

first binding site (Fig. 4b). The loop connecting H2 and H2′, known for being susceptible to posttranslational modification in PPARs,[49] will hereafter be referred to as the P site. In addition to the Ω-loop and the P site, H12 was mildly stabilized by the second ligand, as indicated by the root-mean-square deviation (RMSD) distribution in Fig. 5a, which is slightly narrower and shifted to smaller values in the presence of two ligands. The two-dimensional plots of the RMSD values of H12 *versus* the RMSD of the Ω-loop and the P site (Fig. 5b) indicate that the mobility of H12 correlates directly with the mobility of these two other regions; correlations occur in both systems but are systematically enhanced by the second ligand despite the narrower range of RMSD values with two ligands. No significant changes were

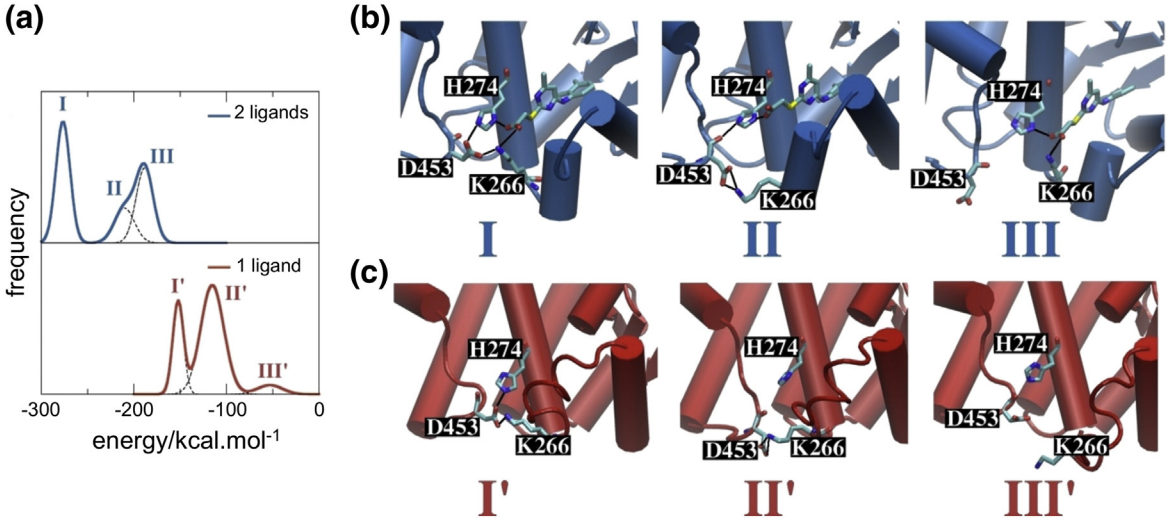

Fig. 6. The charge cluster formed by residues K266, H274 and D453 acts as a bridge connecting the Ω-loop, the loop preceding H12 and the H3. For both systems (one or two ligands), three different modes of interaction were observed within the charge cluster, whose frequency is shown in (a). In the system containing a second ligand molecule (blue), the charge cluster is stabilized as compared to the single ligand case (red). As shown by the representative structures, the charge cluster is stabilized by interactions that involve the second ligand itself (b) and, thus, cannot be fully formed in its absence (c).

observed in the structure or dynamics of other regions of PPARα LBD, supporting the idea that the second WY14643 only strongly stabilizes the Ω-loop and the P site and indirectly promotes a more subtle stabilization of H12.

Close inspection of the MD trajectories indicates that stabilization of Ω-loop and H12, as well as the correlation between their mobilities, can be partially explained by electrostatic interactions involving H274 (H3), K266 (Ω-loop) and D453 (loop H11–H12). In both systems (with one or two ligands), these residues may form similar salt bridges that comprise the charge cluster connecting the Ω-loop, the loop preceding the H12 and the H3 (Fig. 6). In the presence of a single ligand (Fig. 6a, lower panel, and c), at least three different interaction modes within this charge cluster were identified. Modes I′ and II′ are characterized by average interaction energies of −152.2 ± 5.8 kcal/mol (44% of the simulation time) and −115.3 ± 12.5 kcal/mol (52% of simulation time), respectively, and both connect the Ω-loop to the loop preceding H12. Mode III′ (no bridge) is enthalpically less favorable, with an average energy of only −53.1 ± 13.4 kcal/mol. Mode III′ appears only 4% of the simulation time.

Electrostatic interactions in the second binding site are more frequently formed in the presence of the second ligand, with the ligand itself participating in the charge cluster (Fig. 6a, top panel, and b). Interaction modes are similar to those occurring in the presence of a single ligand but are more stable because of the additional interactions provided by the second ligand itself. Mode I that represents the most stable form of the charge cluster—with four different interactions occurring simultaneously—is also the most frequently sampled mode, appearing in 52% of the simulation time. Interestingly, the interactions occurring in mode I connect the Ω-loop not only to the loop preceding H12 but also to H3. Mode II appears less frequently (22% of the simulation time), but like mode I, it displays interactions that connect the Ω-loop to the loop preceding H12. Mode III (29%) resembles mode III′ since it does not directly connect the Ω-loop to the loop preceding H12. However, mode III displays two interactions connecting the highly mobile Ω-loop and H3, as in mode I.

Among these interactions, we propose that the K266–D453 salt bridge is at least partially responsible for the observed correlations between mobilities of the Ω-loop and H12 since it provides direct contact between this loop and the loop preceding H12. Moreover, this interaction is frequently formed in both systems (modes I, I′, II and II′). Alone, however, this salt bridge might enhance H12 mobility by connecting it to the highly mobile Ω-loop. It may, therefore, account for the correlation between these two regions but not for ligand-induced stabilization of H12 observed during the course of the simulations. Instead, we attribute the additional stabilization of H12 to interactions that directly or indirectly connect the highly mobile Ω-loop to H3, one of the most rigid regions of PPARα LBD, as already shown in Fig. 4. Apart from the previously mentioned hydrophobic contacts, there are important second ligand-mediated electrostatic interactions between Ω-loop and H3 exemplified by modes I and III that contribute to H12 stabilization.

Overall, mutagenesis experiments and dynamic simulations suggest that the salt bridge connecting the Ω-loop to the loop preceding the H12 is important for correlating these two regions, but this correlation only translates into H12 stabilization if the Ω-loop is stabilized by further second ligand-dependent interactions with H3.

WY14643 induced dose-dependent decrease in IL-6 and IL-8

We compared the antiinflammatory activity of WY14643 to that of the PPARα antagonist, GW6471, in a human corneal cell wound-healing model, which simulates exposure to hypertonic tears encountered in some types of dry eye disease. Figure 7 shows that the human corneal epithelial cells (HCEC) cell line expresses PPARα protein. Antibody selectivity was validated by the fact that omission of the primary antibody eliminated staining.

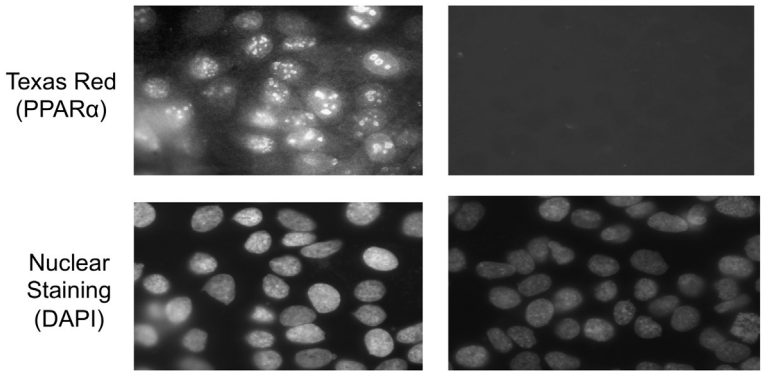

Fig. 7. Immunohistochemistry confirms the presence of PPARα expression in HCEC. Omission of primary antibody confirms selectivity of anti PPARα antibody. Nuclei were stained with 4′,6-diamidino-2-phenylindole.

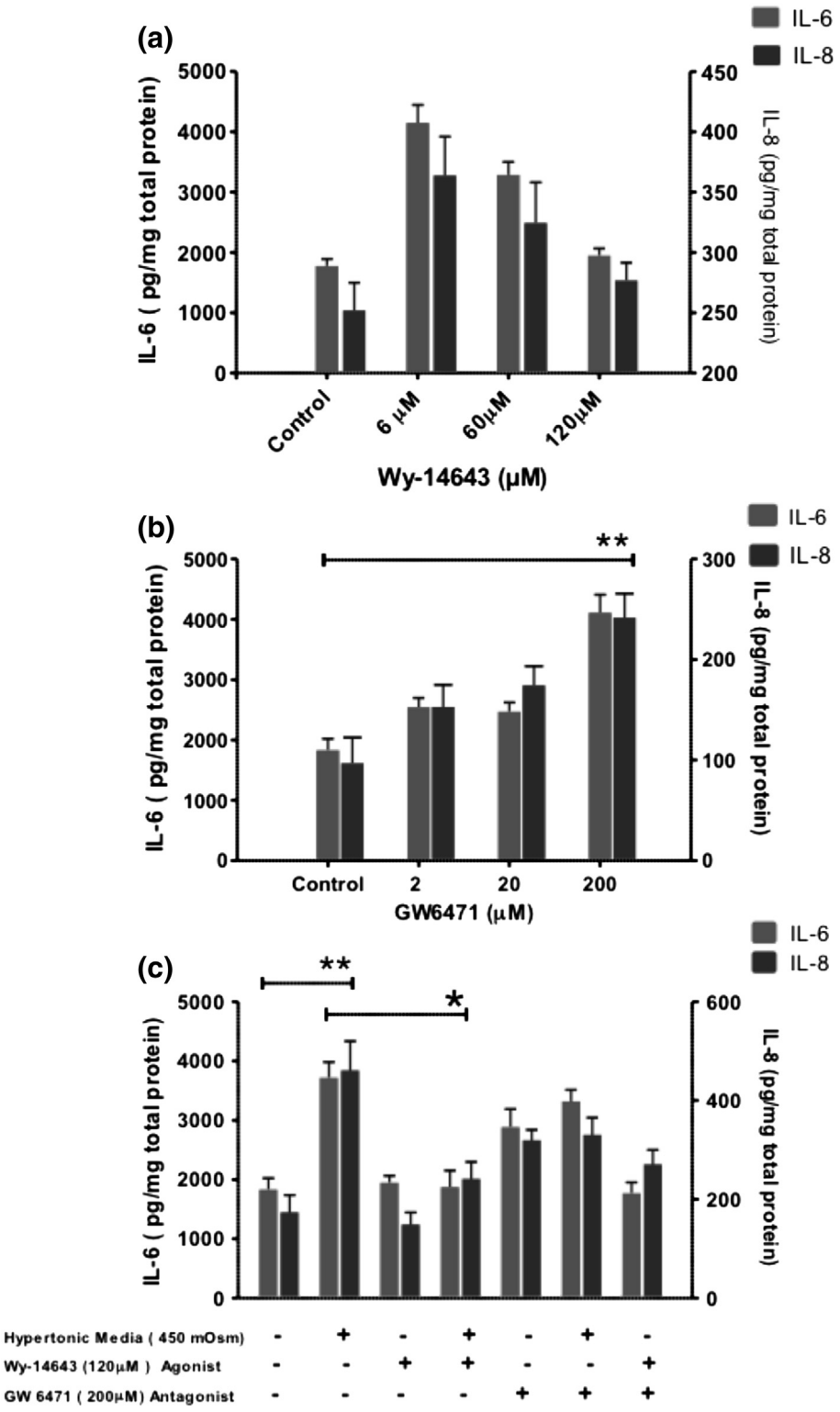

Fig. 8. Changes in IL-6 and IL-8 expression induced by modulation of PPARα activity under hypertonic (i.e., 450 mOsm) and isotonic (i.e., 300 mOsm) conditions. Under isotonic conditions, HCEC were exposed for 24 h to different doses of (a) PPARα agonist WY14643 and (b) PPARα antagonist GW6471. (c) Under hypertonic conditions, HCEC were exposed to different doses of WY14643 and GW6471. Subsequent to incubation, medium was collected and IL-6 and IL-8 levels were assayed by enzyme-linked immunosorbent assay. Data were normalized based on cell density through protein content using a modified Lowry procedure. Each experiment was repeated three times and performed in triplicate on each occasion. Data are expressed as means ± SEM.

HCEC were then subjected to an environmental stress (450 mOsm hypertonic medium) identified in the tears of some dry eye patients. These individuals have elevated expression of two cytokine biomarkers (IL-6 and IL-8) that are also elicited *in vitro*.[50] Such rises contribute ocular inflammation in dry eye patients with aqueous deficient tears.[51]

Under isotonic conditions, the results shown in Fig. 8a indicate that, at doses near the EC_{50} value for WY14643 (i.e., 5.4 μM), IL-6/IL-8 levels were induced to similar levels obtained from those induced by the hypertonic stress (Fig. 8c). However, at the dose needed to maximally activate PPARα, IL-6/IL-8 levels were lowered to near control levels measured in a 300-mOsm isotonic medium. In contrast to this biphasic effect, the PPARα antagonist (GW6471) increased IL-6/IL-8 levels in a strictly dose dependent fashion (Fig. 8b). In NaCl supplemented hypertonic (450 mOsm) Dulbecco's modified Eagle's medium (DMEM)/F12 medium, IL-6/IL-8 levels rose about 2-fold whereas pre-incubation with WY14643 (120 μM) suppressed such rises to near baseline levels measured under isotonic conditions (Fig. 8c). Such suppression was not cytotoxic since the IL-6/IL-8 levels measured, in the presence of WY14643, during exposure to the hypertonic stress were the same as those under the isotonic condition. Figure 8b shows that 200 μM GW6471 enhanced IL-6/IL-8 release by 1.5-fold under both isotonic and hypertonic conditions. These increases in IL-6/IL-8 caused by GW6471 were partially suppressed by pre-incubation with WY14643 (Fig. 8c). Together, opposing effects of WY14643 and GW6471 on IL-6 and IL-8 show that PPARα regulates cytokine expression in HCEC similar to another study employing primary HCEC.[26]

Discussion

WY14643 is a synthetic PPARα ligand that resembles clinically useful fibrate drugs and is often used as a positive control for PPARα activation. Nevertheless, the molecular elements involved in protein–ligand recognition by PPARα were not known. Here, we report a structure of the PPARα in complex with WY14643, which suggests that this fibrate analog induces activation through an unusual bipartite mechanism involving conventional direct H12 stabilization and an alternative mode that involves a second ligand in the pocket.

The first WY14643 ligand copy directly interacts with helix 12, like many other PPAR agonists, and also forms similar interactions with polar residues that are important for stabilizing the majority of known ligands for this protein target. These interactions include the direct contact with Y473 localized in AF-2, which promotes stabilization of the active protein conformation. This configuration also provides additional stabilization of the ligand hydrophobic tail by nonpolar residues in the inner region of the first site. A close-up view of superimposed PPAR subtype structures around the first site reveals PPARα-specific amino acid contacts with the first copy that explain why WY14643 preferentially activates PPARα *versus* other subtypes. This agrees with previous studies revealing the importance of a single residue substitution within this region of the pocket in modulating ligand selectivity.[52,53]

Crystallographic model refinement also identified a second WY14643 molecule within the pocket. Two lines of evidence suggest that this second binding site is important for function. First, mutation analysis of residues that contact the second ligand copy (V255 and I263), but not the first, is required for optimal activity of WY14643 and does not interfere with activity of another PPARα ligand (GW7647) that only occupies the first site. Second, MD simulations suggest that the second ligand strongly stabilizes the highly mobile Ω-loop by the formation of a charge cluster that also involves the ligand itself, and this event appears to be directly correlated with a more subtle stabilization of H12 and the P site. Thus, we suggest that the second site locally stabilizes important regions of the protein that indirectly influence H12.

Similar mechanisms have been proposed to explain actions of PPARγ partial agonists—ligands that lack direct contact with H12 but can still activate PPARγ to a lesser extent—and also bind at a similar location to the second WY14643 site. For these ligands, recent experimental evidence point to alternative mechanisms that do not involve the stabilization of H12, but rather the stabilization of H3 and the β-sheets[54] and/or modifications in the structure and dynamics of the flexible region known as Ω-loop.[55–57] These data suggest that, although the stabilization of alternative regions might not be required for normal activation by ligands that contact H12, it is still important for activation of PPARs by ligands that bind near the β-sheets/Ω-loop and do not interact directly with H12. It is also interesting to propose that PPARα activity modulation by other fibrate analogs might involve partial occupation of the second binding pocket by ligand hydrophobic tails. Alterations in the position of hydrophobic interactions between fibrate extended poly-aryl group and hydrophobic residues within the pocket account for ligand potency variations.[10]

We recognize that our proposed model would be strengthened by direct determination of ligand stoichiometry and affinity for wild-type PPARα and the PPARα second-site mutant (V255A/I263A) by isothermal titration calorimetry. In fact, we attempted these studies, but technical difficulties prevented accurate measurements of ligand binding properties. Specifically, only 5% of our PPARα LBD prepara-

tions were competent to bind ligand and, thus, initial ligand association was extremely rapid with low apparent stoichiometry. We attribute this observation to an extremely high prevalence of bacterial fatty acids within the PPARα ligand binding pocket that prevent binding of other ligands, and we have confirmed the presence of these ligands (predominantly myristic, palmitic and stearic acids) by mass spectroscopic analysis of purified PPARα LBD and crystallization of PPARα in the absence of exogenous ligand (data not shown). We attempted to remove these fatty acids with a variety of chromatographic techniques, without success, and to crystallize the PPARα V255A/I263A mutant to see whether WY14643 occupied the first site, again without success. While it therefore remains possible that our V255A/I263A mutation impairs PPARα function via effects on overall protein stability and not direct effects upon ligand binding at the second site, two lines of evidence argue against this interpretation. First, activity of a ligand that only binds at the first site (GW7647) is completely unaffected by this mutation. Second, WY14643 remains competent to weakly activate PPARα V255A/I263A and we favor the notion that this reflects activity of ligand bound to the first site alone.

Given that several MD studies with RAR,[58] RXR,[59] TR[47,60,61] and PPARs[62] suggested that the Ω-loop constitutes a ligand entry/exit pathway, one may argue that the PPARα V255A/I263A mutation could impair general ligand association processes rather than specifically blocking WY14643 interactions with the second site. However, such a blockage should have similar affect in the association of the ligand GW7647, which displayed full activity in the context of the double-mutated PPARα. Moreover, a decrease in the ligand association rates would be accompanied by a similar decrease in the dissociation rates. Therefore, the putative impairment of ligand association would reduce the activity to the same extend that the impaired dissociation would increase its activity by increasing its residence time in the binding pocket.

Future studies could be performed to refine the identity of the sites within the LBD that need to be ligand bound in order to further optimize binding affinity and functional PPARγ activation. This could be performed through consideration of a larger binding area to be filled, which might result in better ligand affinity and improvement of protein activation. Alternatively, the LBD region could also be interrogated to design novel partial agonists for the purpose of decreasing potential disadvantages of strong agonists. Such an approach has led to the identification of targets on PPARγ for activation by partial agonists.

We have shown that the PPARα agonist WY14643 exhibits antiinflammatory activity in corneal cells subjected to hypertonic stress. Thus, we believe that drug stimulation of PPARα activity may be a viable method to reduce inflammation in dry eye disease. We must approach this idea with caution. Another group investigated effects of PPARα agonists upon inflammation in ocular cells and observed enhancement of IL-6 production, and we obtained similar results with subsaturating WY14643 levels in hypotonic medium. However, stimulatory effects of lower levels of WY14643 were reversed at higher WY14643 concentrations and we also observed strong suppression of IL-6 ad IL-8 production in hypertonic medium. It is likely that the inhibitory effects of WY14643 upon IL-6 and IL-8 production that we observed are PPARα dependent because they were reversed by the PPARα antagonist GW6471. We believe that the likely explanation for apparent discrepancies between our results and those of previous studies lies in the mode of induction; we used hypertonic stress to induce inflammation and applied WY14643 later whereas the other group co-treated cells with IL-1β and PPARα agonist. It is also interesting to speculate that biphasic effects of WY14643 upon inflammatory response could be related to stoichiometry of ligand in the pocket, although we recognize that this idea is far from proven. It will be important to test activity of existing and novel PPARα agonists in a variety of assays to understand how these compounds affect inflammation and whether binding of ligands at different pocket sites could exert differential effects on inflammation.

Based on aforementioned approaches, we surmise that binding of a second WY14643 molecule in another region of the protein pocket plays a critical role in maintaining potent PPARα functional activity. Additionally, this unique binding mode thus provides a new mode of ligand recognition and structural basis of ligand design, offering clues for improving the binding affinity and selectivity of ligand to the target protein.

Experimental Procedures

Expression and purification

The LBD of hPPARα (amino acids 194–468) was expressed in *Escherichia coli* strain BL21 DE3 as an N-terminal histidine tag from the pET28a expression vector, where the protein was cloned. Transformed bacteria were cultured in LB medium with the addition of 50 μg/mL kanamycin at 37 °C. Protein overexpression was induced by addition of 1 mM isopropyl β-D-1-thiogalactopyranoside, and the temperature was shifted to 18 °C. Cells were harvested 12 h after induction and resuspended in 30 mL buffer A [50 mM sodium phosphate buffer (pH 7.5), 300 mM sodium chloride (NaCl) and 10% glycerol] supplemented with 10 mM β-mercaptoethanol, 10 mM

phenylmethylsulfonyl fluoride and 500 μg/mL lysozyme per liter of culture. Then, the lysate was sonicated and clarified by centrifugation, and the supernatant was loaded onto a Talon Metal Affinity Resin (BD Biosciences Clontech, Palo Alto, CA). After extensive washing of column with buffer A, hPPARα LBD was eluted with buffer B [50 mM sodium phosphate buffer (pH 7.5), 300 mM NaCl, 10% glycerol, 300 mM imidazole and 10 mM β-mercaptoethanol]. A second step of purification was included, using gel-filtration chromatography on a HiLoad 16/60 Superdex 75 column (GE Healthcare) equilibrated with buffer C [20 mM Hepes (pH 8.0), 150 mM NaCl, 5% glycerol and 1 mM dithiothreitol]. Fractions containing the protein of interest were pooled, the N-terminal His tag was cleaved with thrombin protease (0.5 U/mg of protein) and the purity of hPPARα LBD (>95%) was analyzed by Coomassie Blue Stained SDS-PAGE.

Crystallization and data collection

Crystals of hPPARα LBD + WY14643 complex were obtained by co-crystallization. Concentrated samples of purified protein (hPPARα LBD at 10 mg/mL) were mixed with 1 mM WY14643 in order to form the complexes. The initial screening of crystallization conditions was performed using a HoneyBee crystallization robot 931 (Genomic Solutions), and the conditions that seemed promising were reproduced using hanging-drop vapor-diffusion method in the traditional manual setup in which 1-μL hPPARα LBD + WY14643 samples were mixed with an equal volume of reservoir solution and equilibrated against 500-μL reservoir solution. Crystals were obtained in a few days during exposure to a reservoir solution whose composition was 100 mM Tris–HCl (pH 7.5) and 30% (w/v) polyethylene glycol 10,000 at 18 °C. After briefly soaking in a cryoprotective solution [crystallization condition with the addition of 15% (v/v) ethylene glycol], the crystals were flash-cooled in a gaseous nitrogen stream at 100 K and the X-ray diffraction data set was collected at the protein crystallography MX2 beamline at the Laboratório Nacional de Luz Síncroton (Campinas, Brazil) using synchrotron radiation of wavelength 1.459 Å and MAR225 mosaic detector, with an oscillation of 0.25° per frame. Data reduction and integration were performed using iMOSFLM[63] and scaled using SCALA.[64] Statistics of data collection are given in Table 1.

Model refinement and structure determination

The structure model was constructed by molecular replacement using the program PHASER[64] and PDB ID 2REW as template. The programs PHENIX[29,65] and Coot[66] were used to alternately run cycles of model building and refinement. The ligand and water molecules were included only in the last steps of refinement. Refinement statistics are given in the Table 1. The atomic coordinates and structure factors of hPPARα LBD + WY14643 crystal structure reported here were deposited in the PDB under code 4BCR.

Site-directed mutagenesis

The mutagenesis experiments were carried out according to Batista *et al*. and the manufacturer's protocol provided by QuikChange Site-Directed Mutagenesis Kit (Stratagene).[67] The mutated residues were chosen by inspection of the crystallographic structure and introduced by PCR in the existing vector pBIND, containing hPPARα LBD/GAL4 DBD chimeric protein, by overlapping of mutated primers. All mutated constructs were verified by sequencing.

Transient co-transfection assays

Transactivation assays using luciferase gene reporter were carried out following transient transfection of three plasmids: pGRE-LUC (GAL4 responsive element, *Firefly* luciferase reporter vector), pBIND plasmid (Promega) containing wild type or mutants of hPPARα LBD/GAL4 DBD chimeric protein and pRL plasmid (Promega) containing the *Renilla* luciferase gene, included as a transfection and cell viability control. These plasmids were transfected using FuGENE 6 transfection reagent (Roche), according to the manufacturer's protocol, in the HepG2 cells (from the Cell Culture Facility at the University of California, San Francisco) cultured in DMEM supplemented with 10% (v/v) fetal bovine serum, 4 mmol/L glutamine, 100 U/mL penicillin and 0.1 g/L streptomycin, under 95% air and 5% CO_2 at 37 °C.[68] To perform the assays, we plated the cells in a 24-well plate (density of 1.2×10^5 cells/well) and, after 24 h of transfection, we added the ligands to the cells at the indicated concentrations to construct the dose–response curves. The cells were lysed for another 24 h after the onset of stimulation using the lysis buffer (Dual-Luciferase Report Assay System; Promega). The constant light signal reporter gene assay was performed in a Safire 2 luminescent counter (Tecan, Tecan US, Durham, NC) and the relative luminescence of *Firefly* luciferase activity was normalized to the *Renilla* luciferase activity. Obtained data were fitted using a sigmoidal dose–response function with corresponding EC_{50} determination according to GraphPad Prism software (version 5.0).

MD simulations

The initial configuration for the PPARα LBD complex was obtained from the crystallographic structure reported here. The complete simulated systems were built with VMD (solvate and autoionize plugins)[69] containing the PPARα LBD complex, including protein, ligands and structural water molecules, as well as solvent and counterions for electroneutrality at the physiological concentration (0.15 M). We used a simulation box of dimensions 72.92 Å × 86.21 Å × 86.83 Å containing 15,300 water molecules and 22 pairs of Na^+ and Cl^- ions for simulations with a single WY14643 ligand. An extra Na^+ ion was added in the simulations with two ligands. The average thickness of the protein hydration layer was 15 Å. The H^{++} server was used to set the protonation state of the acid and alkaline residues.[70] Arginines, lysines, histidines and glutamic and aspartic acids were considered in their ionic state, with exception of histidines H396, H406, H440 and H457, which were considered neutral (epsilon hydrogen). Auxiliary simulations were also conducted with deprotonated H274, yielding essentially identical results as with the neutral state of this residue.

The MD simulations were performed using a time step of 2.0 fs and the velocity Verlet algorithm.[71] A 14-Å cutoff with smooth switching function starting at 12 Å was used for the van der Waals interactions, whereas electrostatic forces were treated via the particle mesh Ewald method.[72] Minimization and equilibration were performed as follows: the energy of the system was minimized by 2000 conjugate gradient steps followed by 200 ps equilibration MD simulation in the NPT ensemble keeping all protein atoms fixed. Fixing only the C^{α} atoms, we performed another 2000 conjugate gradient steps and 200 ps equilibration MD simulation. Finally, 2 ns equilibration MD simulations were carried out without any restrictions. Temperature and pressure were kept constant at 298 K and 1 bar with Langevin thermostat and barostat. The damping coefficient of Langevin thermostat was 5 ps^{-1}. The oscillation period and decay time of the piston in Langevin barostat was 200 fs and 100 fs, respectively. The production MD simulations were performed after this protocol in the NPT ensemble, lasting 6 ns.

Using this procedure, we carried out six independent simulations for each one of the systems described as follows: (i) PPARα LBD bound to two ligands (one in the classical ligand binding pocket and the other in the second binding site) and (ii) PPARα LBD bound to only one ligand (in the classical ligand binding pocket). All simulations were performed with NAMD 2.8[73] applying the CHARMM 27 force field for proteins[74] and the TIP3P model for water.[75] The WY14643 molecule was parameterized consistently with the CHARMM force field following the protocol used for other biomolecules.[76,77]

Trajectory analyses, including RMSF, RMSD and interaction energies, were performed using VMD[69] and homemade analysis programs. We also used a homemade program to perform principal component analysis (PCA) on the MD trajectories. Briefly, the PCA method allows one to decompose the dynamics of the protein into several independent (orthonormal) motions, each one describing part of the total motion of the system.[78] Apart from providing a better understanding of the main motions described by the protein, PCA makes it possible to combine only the motions of higher amplitudes in a trajectory to describe the so-called essential dynamics of the system. We applied PCA to our set of MD trajectories, and the resulting "essential trajectories" composed of the first three principal components were used to interpret some aspects of protein dynamics reported here.

Immunostaining assays

SV40 HCEC kindly supplied by Araki-Sasaki were maintained in DMEM/F-12 supplemented with 6% fetal bovine serum, 5 ng/mL epidermal growth factor, 5 μg/mL insulin and 40 μg/mL gentamicin in humidified 5% CO_2, 95% ambient air incubator at 37 °C.[79] Cells were grown to 80–90% confluence in DMEM with supplements in a 50-mm flask (Corning). Cells were detached with 0.5% trypsin ethylenediaminetetraacetic acid and were subcultured in DMEM/F12 medium in a 12- or 24-well plate with appropriate amount of medium. Cell cycle arrest was achieved by culturing cells in serum-free and epidermal growth factor-free DMEM/F-12 medium overnight before optimization of cell responsiveness.

HCEC were immunostaining following being fixed on ice for 15 min with 1% paraformaldehyde–phosphate-buffered saline (PBS) solution and washed three times with Hepes Ringer solution and permeabilized with 0.1% Triton in PBS for 20 min and then washed. Normal goat serum (10%) was used to block nonspecific cell binding sites for 30 min. The cell monolayers were exposed overnight at 4 °C to a primary antibody (i.e., rabbit anti-PPRAα polyclonal IgG) at a dilution of 1:200 (in 1.5% goat serum/PBS solution). After three-time washes with Hepes Ringer solution, the cell monolayer was incubated with a secondary antibody (i.e., rabbit anti-PPAR anti-rabbit IgG-TR at a dilution of 1:800 for 30 min at room temperature). The HCEC were then loaded with a nuclear dye, 1 μM SYTO®16, for 5 min and then washed with Hepes Ringer solution. Images were taken with a Nikon inverted microscope with a 60× objective lens (N.A. 1.4) and with a Roper Scientific CCD camera and images were processed using Photoshop 5.5 (Adobe Systems, San Jose, CA).

Enzyme-linked immunosorbent assay

IL-6 and IL-8 content was determined in the supernatants using enzyme-linked immunosorbent assay (R&D Systems, Minneapolis, MN) according to the manufacturer's instructions. HCEC were plated in 12-well cell culture plates to reach 80–90% confluence and exposed to WY14643 or PPARα antagonist (GW6471) for 30 min before stressing them with NaCl supplemented hypertonic (450 mOsm) DMEM/F12 medium for 24 h. Supernatants were harvested after centrifugation at 1000 rpm for 5 min to remove cell debris. The supernatants were stored at –80 °C until analysis. Protein concentration of each cell lysate was determined by using a bicinchoninic acid protein assay kit. The amounts of IL-6 and IL-8 in the culture medium were normalized according to the total amount of cellular protein lysed with 5% SDS and 0.5 N NaOH. Results were expressed as mean picograms of IL-6 or IL-8 per milligram of cell protein ± SEM (*s*tandard *e*rror of the *m*ean) ($n = 3$). Data are expressed as mean ± SEM. Experiments were performed in triplicate unless otherwise indicated. Statistical significance was determined by Student's unpaired *t*-test. $P < 0.05$ was taken to be significant unless otherwise stated.

Supplementary data to this article can be found online at http://dx.doi.org/10.1016/j.jmb.2013.05.010

Accession number

The atomic coordinates and structure factors of hPPARα LBD + WY14643 crystal structure were deposited in the PDB under code 4BCR.

Acknowledgements

We thank Laboratório Nacional de Luz Síncroton (Brazil) for access to the W01B-MX2 beamline and others facilities. This work was supported by

FAPESP (São Paulo Research Foundation) and National Institutes of Health Grant DK41482 to P.W.

Received 26 December 2012;
Received in revised form 30 April 2013;
Accepted 15 May 2013
Available online 21 May 2013

Keywords:
PPARα;
crystal structure;
protein and ligand interaction;
dry eye disease;
molecular dynamics

Abbreviations used:
PPAR, peroxisome proliferator-activated receptor; DBD, DNA-binding domain; LBD, ligand-binding domain; AF-2, activation function 2; MD, molecular dynamics; RMSF, root-mean-square fluctuation; PBS, phosphate-buffered saline; PCA, principal component analysis; PDB, Protein Data Bank; DMEM, Dulbecco's modified Eagle's medium; HCEC, human corneal epithelial cells.

References

1. Berger, J. & Moller, D. E. (2002). The mechanisms of action of PPARs. *Annu. Rev. Med.* **53**, 409–435.
2. Moore, J. T., Collins, J. L. & Pearce, K. H. (2006). The nuclear receptor superfamily and drug discovery. *ChemMedChem*, **1**, 504–523.
3. Brélivet, Y., Rochel, N. & Moras, D. (2011). Structural analysis of nuclear receptors: from isolated domains to integral proteins. *Mol. Cell. Endocrinol.* **348**, 466–473.
4. Perissi, V. & Rosenfeld, M. G. (2005). Controlling nuclear receptors: the circular logic of cofactor cycles. *Nat. Rev., Mol. Cell Biol.* **6**, 542–554.
5. Bulynko, Y. A. & O'Malley, B. W. (2010). Nuclear receptor coactivators: structural and functional biochemistry. *Biochemistry*, **50**, 313–328.
6. Michalik, L., Auwerx, J., Berger, J., Chatterjee, V., Glass, C., Gonzalez, F. *et al.* (2006). International Union of Pharmacology. LXI. Peroxisome proliferator-activated receptors. *Pharmacol. Rev.* **58**, 726–741.
7. Filip-Ciubotaru, F., Foia, L., Manciuc, C. & Grigore, C. (2011). PPARs: structure, mechanisms of action and control. Note I. *Rev. Med.-Chir. Soc. Med. Nat. Iasi*, **115**, 477–484.
8. Duval, C., Müller, M. & Kersten, S. (2007). PPARα and dyslipidemia. *Biochim. Biophys. Acta*, **1771**, 961–971.
9. van Raalte, D. H., Li, M., Pritchard, P. H. & Wasan, K. M. (2004). Peroxisome proliferator-activated receptor (PPAR)-α: a pharmacological target with a promising future. *Pharmacol. Res.* **21**, 1531–1538.
10. Lannutti, F., Marrone, A. & Re, N. (2011). Prediction of the PPARα agonism of fibrates by combined MM-docking approaches. *J. Mol. Graphics Modell.* **29**, 865–875.
11. Bourguet, W., Germain, P. & Gronemeyer, H. (2000). Nuclear receptor ligand-binding domains: three-dimensional structures, molecular interactions and pharmacological implications. *Trends Pharmacol. Sci.* **21**, 381–388.
12. Samarasinghe, S. P., Sutanto, M. M., Danos, A. M., Johnson, D. N., Brady, M. J. & Cohen, R. N. (2009). Altering PPARγ ligand selectivity impairs adipogenesis by thiazolidinediones but not hormonal inducers. *Obesity (Silver Spring)*, **17**, 965–972.
13. Kota, B., Huang, T. & Roufogalis, B. (2005). An overview on biological mechanisms of PPARs. *Pharmacol. Res.* **51**, 85–94.
14. Desvergne, B. & Wahli, W. (1999). Peroxisome proliferator-activated receptors: nuclear control of metabolism. *Endocr. Rev.* **20**, 649–688.
15. Kersten, S., Desvergne, B. & Wahli, W. (2000). Roles of PPARs in health and disease. *Nature*, **405**, 421–424.
16. Staels, B., Maes, M. & Zambon, A. (2008). Fibrates and future PPARα agonists in the treatment of cardiovascular disease. *Nat. Clin. Pract. Cardiovasc. Med.* **5**, 542–553.
17. Grundy, S. M., Vega, G. L., Yuan, Z., Battisti, W. P., Brady, W. E. & Palmisano, J. (2005). Effectiveness and tolerability of simvastatin plus fenofibrate for combined hyperlipidemia (the SAFARI trial). *Am. J. Cardiol.* **95**, 462–468.
18. Li, J., Kennedy, L. J., Shi, Y., Tao, S., Ye, X. Y., Chen, S. Y. *et al.* (2010). Discovery of an oxybenzylglycine based peroxisome proliferator activated receptor α selective agonist 2-((3-((2-(4-chlorophenyl)-5-methyloxazol-4-yl)methoxy)benzyl)(methoxycarbonyl)amino)acetic acid (BMS-687453). *J. Med. Chem.* **53**, 2854–2864.
19. Santilli, A. A., Scotese, A. C. & Tomarelli, R. M. (1974). A potent antihypercholesterolemic agent: (4-chloro-6-(2,3-xylidino)-2-pyrimidinylthio) acetic acid (Wy-14643). *Experientia*, **30**, 1110–1111.
20. Reddy, J. K., Warren, J. R., Reddy, M. K. & Lalwani, N. D. (1982). Hepatic and renal effects of peroxisome proliferators: biological implications. *Ann. N. Y. Acad. Sci.* **386**, 81–110.
21. Briguglio, E., Di Paola, R., Paterniti, I., Mazzon, E., Oteri, G., Cordasco, G. & Cuzzocrea, S. (2010). WY-14643, a potent peroxisome proliferator activator receptor-α PPAR-α agonist ameliorates the inflammatory process associated to experimental periodontitis. *PPAR Res.* **2010**, 193019.
22. Delerive, P., Fruchart, J. C. & Staels, B. (2001). Peroxisome proliferator-activated receptors in inflammation control. *J. Endocrinol.* **169**, 453–459.
23. Kleemann, R., Verschuren, L., de Rooij, B. J., Lindeman, J., de Maat, M. M., Szalai, A. J. *et al.* (2004). Evidence for anti-inflammatory activity of statins and PPARα activators in human C-reactive protein transgenic mice *in vivo* and in cultured human hepatocytes *in vitro*. *Blood*, **103**, 4188–4194.
24. Devchand, P. R., Keller, H., Peters, J. M., Vazquez, M., Gonzalez, F. J. & Wahli, W. (1996). The PPARα-leukotriene B4 pathway to inflammation control. *Nature*, **384**, 39–43.
25. Saika, S. (2007). Yin and yang in cytokine regulation of corneal wound healing: roles of TNF-α. *Cornea*, **26**, S70–S74.
26. Zhang, J. Z. & Ward, K. W. (2010). WY-14 643, a selective PPARα agonist, induces proinflammatory

and proangiogenic responses in human ocular cells. *Int. J. Toxicol.* **29**, 496–504.
27. Bonazzi, A., Mastyugin, V., Mieyal, P. A., Dunn, M. W. & Laniado-Schwartzman, M. (2000). Regulation of cyclooxygenase-2 by hypoxia and peroxisome proliferators in the corneal epithelium. *J. Biol. Chem.* **275**, 2837–2844.
28. Nolte, R., Wisely, G., Westin, S., Cobb, J., Lambert, M., Kurokawa, R. *et al.* (1998). Ligand binding and co-activator assembly of the peroxisome proliferator-activated receptor-γ. *Nature*, **395**, 137–143.
29. Adams, P. D., Afonine, P. V., Bunkóczi, G., Chen, V. B., Davis, I. W., Echols, N. *et al.* (2010). PHENIX: a comprehensive Python-based system for macromolecular structure solution. *Acta Crystallogr., Sect. D: Biol. Crystallogr.* **66**, 213–221.
30. Grether, U., Bénardeau, A., Benz, J., Binggeli, A., Blum, D., Hilpert, H. *et al.* (2009). Design and biological evaluation of novel, balanced dual PPARα/γ agonists. *ChemMedChem*, **4**, 951–956.
31. Xu, H. E., Lambert, M. H., Montana, V. G., Plunket, K. D., Moore, L. B., Collins, J. L. *et al.* (2001). Structural determinants of ligand binding selectivity between the peroxisome proliferator-activated receptors. *Proc. Natl Acad. Sci. USA*, **98**, 13919–13924.
32. Bénardeau, A., Benz, J., Binggeli, A., Blum, D., Boehringer, M., Grether, U. *et al.* (2009). Aleglitazar, a new, potent, and balanced dual PPARα/γ agonist for the treatment of type II diabetes. *Bioorg. Med. Chem. Lett.* **19**, 2468–2473.
33. Lehmann, J. M., Lenhard, J. M., Oliver, B. B., Ringold, G. M. & Kliewer, S. A. (1997). Peroxisome proliferator-activated receptors α and γ are activated by indomethacin and other non-steroidal anti-inflammatory drugs. *J. Biol. Chem.* **272**, 3406–3410.
34. Hsu, M. H., Palmer, C. N., Griffin, K. J. & Johnson, E. F. (1995). A single amino acid change in the mouse peroxisome proliferator-activated receptor α alters transcriptional responses to peroxisome proliferators. *Mol. Pharmacol.* **48**, 559–567.
35. Shipley, J. M., Hurst, C. H., Tanaka, S. S., DeRoos, F. L., Butenhoff, J. L., Seacat, A. M. & Waxman, D. J. (2004). trans-activation of PPARα and induction of PPARα target genes by perfluorooctane-based chemicals. *Toxicol. Sci.* **80**, 151–160.
36. Lo Verme, J., Fu, J., Astarita, G., La Rana, G., Russo, R., Calignano, A. & Piomelli, D. (2005). The nuclear receptor peroxisome proliferator-activated receptor-α mediates the anti-inflammatory actions of palmitoylethanolamide. *Mol. Pharmacol.* **67**, 15–19.
37. Jin, L., Lin, S., Rong, H., Zheng, S., Jin, S., Wang, R. & Li, Y. (2011). Structural basis for iloprost as a dual peroxisome proliferator-activated receptor α/δ agonist. *J. Biol. Chem.* **286**, 31473–31479.
38. Rau, O., Syha, Y., Zettl, H., Kock, M., Bock, A. & Schubert-Zsilavecz, M. (2008). α-Alkyl substituted pirinixic acid derivatives as potent dual agonists of the peroxisome proliferator activated receptor α and γ. *Arch. Pharm. (Weinheim, Ger.)*, **341**, 191–195.
39. Sierra, M. L., Beneton, V., Boullay, A. B., Boyer, T., Brewster, A. G., Donche, F. *et al.* (2007). Substituted 2-[(4-aminomethyl)phenoxy]-2-methylpropionic acid PPARα agonists. 1. Discovery of a novel series of potent HDLc raising agents. *J. Med. Chem.* **50**, 685–695.
40. Cronet, P., Petersen, J. F., Folmer, R., Blomberg, N., Sjöblom, K., Karlsson, U. *et al.* (2001). Structure of the PPARα and -γ ligand binding domain in complex with AZ 242; ligand selectivity and agonist activation in the PPAR family. *Structure*, **9**, 699–706.
41. Wang, W., Devasthale, P., Farrelly, D., Gu, L., Harrity, T., Cap, M. *et al.* (2008). Discovery of azetidinone acids as conformationally-constrained dual PPARα/γ agonists. *Bioorg. Med. Chem. Lett.* **18**, 1939–1944.
42. Oyama, T., Toyota, K., Waku, T., Hirakawa, Y., Nagasawa, N., Kasuga, J. I. *et al.* (2009). Adaptability and selectivity of human peroxisome proliferator-activated receptor (PPAR) pan agonists revealed from crystal structures. *Acta Crystallogr., Sect. D: Biol. Crystallogr.* **65**, 786–795.
43. Oon Han, H., Kim, S. H., Kim, K. H., Hur, G. C., Joo Yim, H., Chung, H. K. *et al.* (2007). Design and synthesis of oxime ethers of α-acyl-β-phenylpropanoic acids as PPAR dual agonists. *Bioorg. Med. Chem. Lett.* **17**, 937–941.
44. Ambrosio, A., Dias, S., Polikarpov, I., Zurier, R., Burstein, S. & Garratt, R. (2007). Ajulemic acid, a synthetic nonpsychoactive cannabinoid acid, bound to the ligand binding domain of the human peroxisome proliferator-activated receptor γ. *J. Biol. Chem.* **282**, 18625–18633.
45. Amato, A. A., Rajagopalan, S., Lin, J. Z., Carvalho, B. M., Figueira, A. C., Lu, J. *et al.* (2012). GQ-16, a novel peroxisome proliferator-activated receptor γ (PPARγ) ligand, promotes insulin sensitization without weight gain. *J. Biol. Chem.* **287**, 28169–28179.
46. Liberato, M. V., Nascimento, A. S., Ayers, S. D., Lin, J. Z., Cvoro, A., Silveira, R. L. *et al.* (2012). Medium chain fatty acids are selective peroxisome proliferator activated receptor (PPAR) γ activators and pan-PPAR partial agonists. *PLoS One*, **7**, e36297.
47. Martínez, L., Polikarpov, I. & Skaf, M. S. (2008). Only subtle protein conformational adaptations are required for ligand binding to thyroid hormone receptors: simulations using a novel multipoint steered molecular dynamics approach. *J. Phys. Chem. B*, **112**, 10741–10751.
48. Silveira, R. L., Martínez, J., Skaf, M. S. & Martínez, L. (2012). Enzyme microheterogeneous hydration and stabilization in supercritical carbon dioxide. *J. Phys. Chem. B*, **116**, 5671–5678.
49. Berrabah, W., Aumercier, P., Lefebvre, P. & Staels, B. (2011). Control of nuclear receptor activities in metabolism by post-translational modifications. *FEBS Lett.* **585**, 1640–1650.
50. Pan, Z., Wang, Z., Yang, H., Zhang, F. & Reinach, P. S. (2011). TRPV1 activation is required for hypertonicity-stimulated inflammatory cytokine release in human corneal epithelial cells. *Invest. Ophthalmol. Visual Sci.* **52**, 485–493.
51. Na, K. S., Mok, J. W., Kim, J. Y., Rho, C. R. & Joo, C. K. (2012). Correlations between tear cytokines, chemokines, and soluble receptors and clinical severity of dry eye disease. *Invest. Ophthalmol. Visual Sci.* **53**, 5443–5450.
52. Martínez, L., Nascimento, A. S., Nunes, F. M., Phillips, K., Aparicio, R., Dias, S. M. *et al.* (2009).

Gaining ligand selectivity in thyroid hormone receptors via entropy. *Proc. Natl Acad. Sci. USA*, **106**, 20717–20722.
53. Bleicher, L., Aparicio, R., Nunes, F. M., Martinez, L., Gomes Dias, S. M., Figueira, A. C. *et al.* (2008). Structural basis of GC-1 selectivity for thyroid hormone receptor isoforms. *BMC Struct. Biol.* **8**, 8.
54. Bruning, J. B., Chalmers, M. J., Prasad, S., Busby, S. A., Kamenecka, T. M., He, Y. *et al.* (2007). Partial agonists activate PPARγ using a helix 12 independent mechanism. *Structure*, **15**, 1258–1271.
55. Waku, T., Shiraki, T., Oyama, T., Fujimoto, Y., Maebara, K., Kamiya, N. *et al.* (2009). Structural insight into PPARγ activation through covalent modification with endogenous fatty acids. *J. Mol. Biol.* **385**, 188–199.
56. Waku, T., Shiraki, T., Oyama, T. & Morikawa, K. (2009). Atomic structure of mutant PPARγ LBD complexed with 15d-PGJ2: novel modulation mechanism of PPARγ/RXRα function by covalently bound ligands. *FEBS Lett.* **583**, 320–324.
57. Puhl, A. C., Bernardes, A., Silveira, R. L., Yuan, J., Campos, J. L., Saidemberg, D. M. *et al.* (2012). Mode of peroxisome proliferator-activated receptor γ activation by luteolin. *Mol. Pharmacol.* **81**, 788–799.
58. Blondel, A., Renaud, J. P., Fischer, S., Moras, D. & Karplus, M. (1999). Retinoic acid receptor: a simulation analysis of retinoic acid binding and the resulting conformational changes. *J. Mol. Biol.* **291**, 101–115.
59. Carlsson, P., Burendahl, S. & Nilsson, L. (2006). Unbinding of retinoic acid from the retinoic acid receptor by random expulsion molecular dynamics. *Biophys. J.* **91**, 3151–3161.
60. Martínez, L., Webb, P., Polikarpov, I. & Skaf, M. S. (2006). Molecular dynamics simulations of ligand dissociation from thyroid hormone receptors: evidence of the likeliest escape pathway and its implications for the design of novel ligands. *J. Med. Chem.* **49**, 23–26.
61. Martínez, L., Sonoda, M. T., Webb, P., Baxter, J. D., Skaf, M. S. & Polikarpov, I. (2005). Molecular dynamics simulations reveal multiple pathways of ligand dissociation from thyroid hormone receptors. *Biophys. J.* **89**, 2011–2023.
62. Genest, D., Garnier, N., Arrault, A., Marot, C., Morin-Allory, L. & Genest, M. (2008). Ligand-escape pathways from the ligand-binding domain of PPARγ receptor as probed by molecular dynamics simulations. *Eur. Biophys. J.* **37**, 369–379.
63. Leslie, A. (2006). The integration of macromolecular diffraction data. *Acta Crystallogr., Sect. D: Biol. Crystallogr.* **62**, 48–57.
64. Collaborative Computational Project, N. m. (1994). The CCP4 suite: programs for protein crystallography. *Acta Crystallogr., Sect. D: Biol. Crystallogr.* **50**, 760–763.
65. Adams, P., Grosse-Kunstleve, R., Hung, L., Ioerger, T., McCoy, A., Moriarty, N. *et al.* (2002). PHENIX: building new software for automated crystallographic structure determination. *Acta Crystallogr., Sect. D: Biol. Crystallogr.* **58**, 1948–1954.
66. Emsley, P. & Cowtan, K. (2004). Coot: model-building tools for molecular graphics. *Acta Crystallogr., Sect. D: Biol. Crystallogr.* **60**, 2126–2132.
67. Batista, F. A., Trivella, D. B., Bernardes, A., Gratieri, J., Oliveira, P. S., Figueira, A. C. *et al.* (2012). Structural insights into human peroxisome proliferator activated receptor δ (PPAR-δ) selective ligand binding. *PLoS One*, **7**, e33643.
68. Yuan, C., Lin, J. Z., Sieglaff, D. H., Ayers, S. D., Denoto-Reynolds, F., Baxter, J. D. & Webb, P. (2012). Identical gene regulation patterns of T3 and selective thyroid hormone receptor modulator GC-1. *Endocrinology*, **153**, 501–511.
69. Humphrey, W., Dalke, A. & Schulten, K. (1996). VMD: visual molecular dynamics. *J. Mol. Graphics*, **14**, 27–28.
70. Gordon, J. C., Myers, J. B., Folta, T., Shoja, V., Heath, L. S. & Onufriev, A. (2005). H++: a server for estimating pK_as and adding missing hydrogens to macromolecules. *Nucleic Acids Res.* **33**, W368–W371.
71. Verlet, L. (1967). Computer experiments on classical fluids. I Thermodinamical properties of Lennard-Jones molecules. *Phys. Rev.* **21**, 1531–1538.
72. Darden, T., York, D. & Pedersen, L. (1993). Particle mesh Ewald: an *N*-log(*N*) method for Ewald sums in large systems. *J. Chem. Phys.* **98**, 10089–10092.
73. Phillips, J. C., Braun, R., Wang, W., Gumbart, J., Tajkhorshid, E., Villa, E. *et al.* (2005). Scalable molecular dynamics with NAMD. *J. Comput. Chem.* **26**, 1781–1802.
74. MacKerell, A. D., Bashford, D., Bellott, M., Dunbrack, R. L., Evanseck, J. D., Field, M. J. *et al.* (1998). All-atom empirical potential for molecular modeling and dynamics studies of proteins. *J. Phys. Chem. B*, **102**, 3586–3616.
75. Jorgensen, W. L., Chandrasekhar, J., Madura, J. D., Impey, R. W. & Klein, M. L. (1983). Comparison of single potential functions for simulating liquid water. *J. Chem. Phys.* **79**, 926–935.
76. Hansson, A., Souza, P. C. T., Silveira, R. L., Matínez, L. & Skaf, M. S. (2011). CHARMM force field parameterization of roziglitazone. *Int. J. Quantum Chem.* **111**, 1346–1354.
77. Prates, É. T., Souza, P. C. T., Pickholz, M. & Skaf, M. S. (2011). CHARMM-based parameterization of neutral articaine—a widely used local anesthetic. *Int. J. Quantum Chem.* **111**, 1339–1345.
78. Amadei, A., Linssen, A. B. M. & Berendsen, H. J. C. (2004). Essential dynamics of proteins. *Proteins: Struct., Funct., Bioinf.* **17**, 412–425.
79. Araki-Sasaki, K., Ohashi, Y., Sasabe, T., Hayashi, K., Watanabe, H., Tano, Y. & Handa, H. (1995). An SV40-immortalized human corneal epithelial cell line and its characterization. *Invest. Ophthalmol. Visual Sci.* **36**, 614–621.